

**Magnetism in cubic manganese-rich Heusler compounds**Lukas Wollmann,<sup>1</sup> Stanislav Chadov,<sup>1</sup> Jürgen Kübler,<sup>2</sup> and Claudia Felser<sup>1</sup><sup>1</sup>*Max-Planck-Institut für Chemische Physik fester Stoffe, Nöthnitzer Strasse 40, 01187 Dresden, Germany*<sup>2</sup>*Institut für Festkörperphysik, Technische Universität Darmstadt, 64289 Darmstadt, Germany*

(Received 23 September 2014; revised manuscript received 25 November 2014; published 9 December 2014)

Manganese-rich Heusler compounds are attracting much interest in the context of spin transfer torque and rare-earth free hard magnets. Here we give a comprehensive overview of the magnetic properties of noncentrosymmetric cubic Mn<sub>2</sub>-based Heusler materials, which are characterized by an antiparallel coupling of magnetic moments on Mn atoms. Such a ferrimagnetic order leads to the emergence of new properties that are absent in ferromagnetic centrosymmetric Heusler structures. In terms of the band structure calculations, we explain the formation of this magnetic order and the Curie temperatures. This overview is intended to establish guidelines for a basic understanding of magnetism in Mn<sub>2</sub>-based Heusler compounds.

DOI: [10.1103/PhysRevB.90.214420](https://doi.org/10.1103/PhysRevB.90.214420)

PACS number(s): 75.50.Gg, 71.15.Nc, 75.10.Lp, 75.30.Et

**I. INTRODUCTION**

Heusler compounds became objects of interest as a class of materials with peculiar transport and magneto-optical properties with the prediction of half-metallicity (gapping in one spin channel) in NiMnSb [1] and Co<sub>2</sub>MnSn [2] in 1983. The whole family of Co<sub>2</sub>YZ compounds has been as considered suitable materials for spintronics devices, and Co<sub>2</sub>Cr<sub>0.6</sub>Fe<sub>0.4</sub>Al has from then on been the pioneering candidate material [3]. The potential of this class has been explored in the context of magnetoresistance applications, such as in giant-magnetoresistance (GMR) and tunnel-magnetoresistance (TMR) devices. Usage as an electrode material for spin injection, where spin polarization is an inevitable prerequisite, and for spintronics applications in general [4] has been realized. Accompanied by the high Curie temperatures shown by many of the compounds in the Co<sub>2</sub>YZ family, the indispensable premises for room-temperature applications are given. On the basis of these premises, TMR ratios of 1900% at low temperatures were accomplished in Co<sub>2</sub>MnSi|MgO|Co<sub>2</sub>MnSi tunnel junctions by Yamamoto *et al.* [5] in 2012. A few proofs of half-metallicity in general [6] and of Heusler alloys particularly [7] have been given in the literature, while experimental proof of half-metallicity in Co<sub>2</sub>YZ Heusler alloys was given just recently by Jourdan *et al.* [8] through spin-polarized photoelectron spectroscopy experiments on Co<sub>2</sub>MnSi thin films. Consequently, simple rules from experimental and theoretical work have been formed to understand the trends in this class of materials, and the Slater-Pauling (SP) behavior of these compounds has been intensively studied [9–11].

Nowadays, another family of Heusler compounds, the class Mn<sub>2</sub>YZ, has attracted considerable attention for implementation as a free magnetic layer in spin-transfer torque devices such as spin-transfer torque random-access memory (STT-MRAM) [12]. In these devices, a spin-polarized current is passed through a hard magnetic layer whose magnetization is switched through transfer of angular momentum [13]. The most famous member of this group of materials is tetragonal Mn<sub>3</sub>Ga [14,15]. Starting from its prediction as a compensated cubic ferrimagnet, much research in the field has been invested to promote the implementation of this compound. The reasons are found in its properties, namely,

a low experimental magnetic moment, high perpendicular magnetocrystalline anisotropy (PMA) owing to its tetragonal structure, and a high Curie temperature of more than 700 K [14,16], which ensures the thermal stability of the stored information. These properties, in combination with affordable constituent elements, make this material most attractive for high-technology utilization.

Despite difficulties in the realization of such devices, other members of the Mn<sub>2</sub>YZ family have demonstrated their potential [12,17]. Recently, the spin-gapless semiconductor Mn<sub>2</sub>CoAl was predicted and realized, unveiling once again the broad variety of effects to be found in Heusler materials. Peculiar transport properties were expected and have been found in such systems, making them promising candidates for room-temperature semiconductor spintronics.

In addition to the above-mentioned materials, the whole family of compounds based on Mn<sub>2</sub>YZ may show striking properties. To optimize these materials, we need a general understanding of how to design compounds with higher spin polarization and achieve compensation of the magnetization in this class. Therefore, we intend to establish guidelines and form simple rules for the Mn<sub>2</sub>YZ family of Heusler compounds.

Here we intend to explain the formation of the total moments through monitoring of the local magnetic structure and its influence on easily accessible, measurable properties such as the Curie temperature. While the existence of several Heusler-derived structure types is well known [14,18–22], the interplay between the structure, magnetism, and local magnetic moments has not been elucidated as yet, in contrast to the intensively studied cobalt-based Heusler alloys. We will present our work based on theoretical methods, i.e., density functional theory, focusing on the local magnetic structure, and the emergence of the magnetic moments on the Mn atoms as the composition is altered. Furthermore, the evaluation of the interatomic exchange in terms of the exchange constant  $J_{ij}$  is essential for understanding the formation of the resulting magnetic order. The influence of the electron count on the magnitude of the total moments, the composing local moments, and the exchange interaction is disentangled. In a later publication, we intend to apply the gathered knowledge to tetragonal Mn-based compounds.

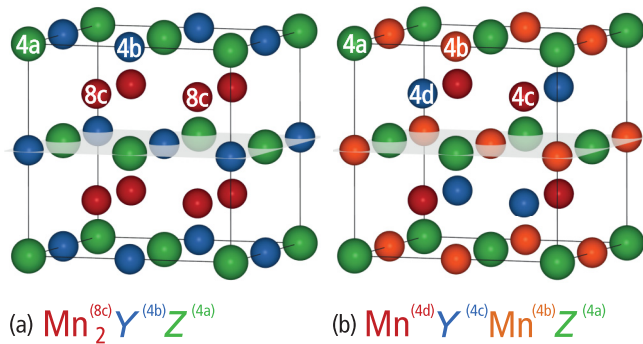


FIG. 1. (Color online) Two basic ordering possibilities for the ternary  $X_2YZ$  composition ( $X$ ,  $Y$  transition metals and  $Z$  main-group element, marked as red, blue, and green, respectively) within the fcc lattice: (a)  $L_{21}$ -type, occupation of  $8c$  by  $X$  and  $4b$  by  $Y$  (“regular” structure); (b)  $X_a$ -type,  $8c$  is split into  $4c$  and  $4d$  sites due to their different occupation (“inverse” structure).

## II. CRYSTAL AND MAGNETIC STRUCTURES

For ordered cubic Heusler materials, two prototypical structure types exist. The so-called “regular” type ( $\text{Cu}_2\text{MnAl}$ ,  $L_{21}$  prototype) crystallizes in spacegroup (SG) 225, with three inequivalent Wyckoff positions ( $8c$ ,  $4b$ , and  $4a$ ) incorporating four atoms per unit cell. These positions are occupied according to the following scheme. The  $8c$  Wyckoff position  $(\frac{1}{4}, \frac{1}{4}, \frac{1}{4})$  is occupied by two Mn atoms, whereby positions  $4b$   $(\frac{1}{2}, \frac{1}{2}, \frac{1}{2})$  and  $4a$   $(0,0,0)$  are filled with  $Y$  and  $Z$  atoms.  $Y$  represents any transition metal (TM) and  $Z$  stands for a main group element. The nearest-neighbor coordination can be seen in Fig. 1(a). Another prototype often appearing in the context of Heusler compounds is the  $\text{Li}_2\text{AgSb}$ -type structure [sometimes named “inverse” Heusler type, Fig. 1(b)], which can be derived from the “regular” Heusler type by interchanging half of the atoms on position  $8c$  with the  $4b$ -position-occupying element. This reduces the symmetry of the cell, leading to spacegroup 216 ( $X_a$ -type) with four inequivalent positions in the unit cell. In this case, these are occupied with Mn at  $4d$   $(\frac{1}{4}, \frac{1}{4}, \frac{1}{4})$ ,  $Y$  at  $4c$   $(\frac{3}{4}, \frac{3}{4}, \frac{3}{4})$ , Mn at  $4b$   $(\frac{1}{2}, \frac{1}{2}, \frac{1}{2})$ , and  $Z$  at  $4a$   $(0,0,0)$ .

The occurrence of these two types of structures for ternary and even quaternary Heusler alloys has been related to a rule of thumb [23], which states for  $X_2YZ$  that (i) the inversion-symmetric  $L_{21}$ -type structure with  $X$  occupying site  $8c$  is favored if  $X$  has a higher valence electron count than  $Y$ . However, (ii) if  $X$  is the earlier transition metal, then the structure lacks inversion symmetry, as site  $8c$  splits into two inequivalent sites,  $4c$  and  $4d$ , which are occupied by  $X$  and  $Y$ , while the second  $X$  is found on site  $4b$ . Intermixing of sites has been reported, leading to disordered structural variants of the initial Heusler structure types [23]. Additional structures in the phase space of Heusler compounds are tetragonal derivatives from the cubic parent phases, which can be obtained from these by elongation or compression of the cell axes.

The family of  $\text{Mn}_2YZ$ -based Heusler systems is relatively new as compared to other groups such as  $\text{Co}_2YZ$ ,  $\text{Fe}_2YZ$ , and  $\text{Ni}_2YZ$ , which have been thoroughly studied over the last few decades. In the context of magnetism, the distinct feature

of  $\text{Mn}_2$  systems is that their magnetization typically does not exceed  $2 \mu_B/\text{f.u.}$  (in certain rare cases it can reach  $4 \mu_B$ ). This is different from the “older” groups, where the magnetization reaches values of  $5\text{--}6 \mu_B/\text{f.u.}$  because those materials are known to exhibit ferromagnetic ordering and to incorporate elements with higher number of valence  $d$  electrons on the  $X$  position ( $\text{Mn}_3\text{Ga}$ :  $N_V = 24$ ,  $M = 0\mu_B$ ;  $\text{Co}_2\text{MnGa}$ :  $N_V = 28$ ,  $M = 4\mu_B$ ), leading to a higher magnetization according to the SP rule. The SP rule for four atoms per formula unit describes the relationship between  $N_V$  of a compound and its measurable magnetic moment, which is given by

$$M = N_V - 24. \quad (1)$$

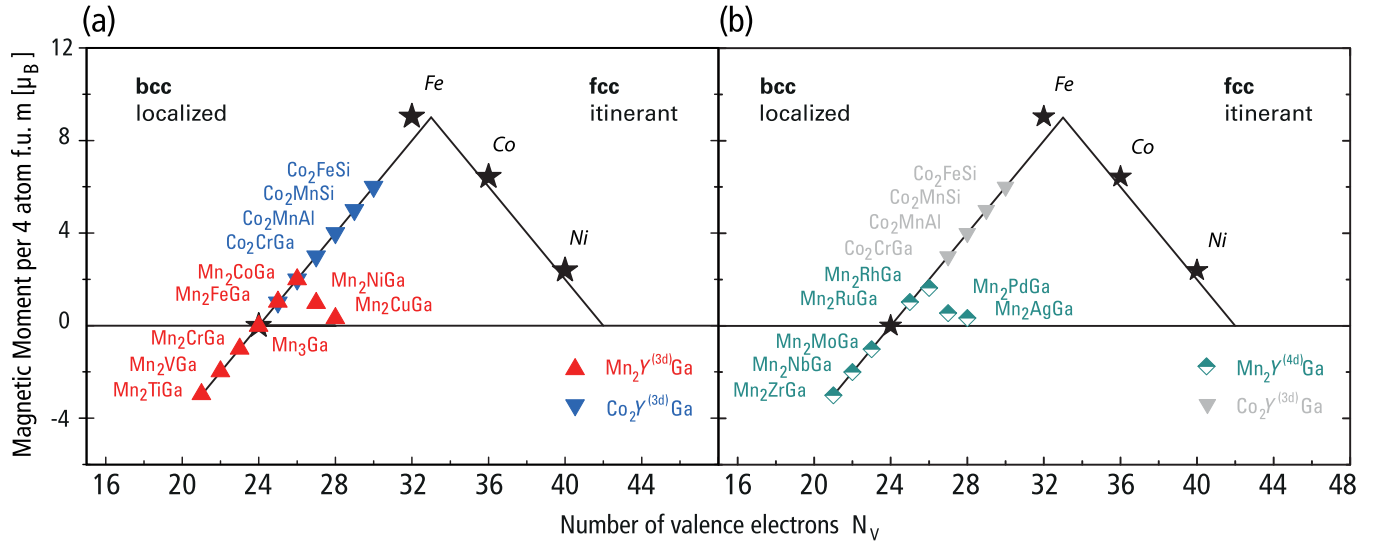
This kind of behavior was first observed for pure  $3d$  transition metals and alloys by Slater, Pauling, and Friedel [24–26], and it was later applied to cubic half-metallic Heusler materials [27]. The description and origin of the SP rule for several Heusler materials was given earlier [11,23,28]. The observable types of magnetic ordering in the  $\text{Mn}_2YZ$ -based Heusler family will be part of this work and will be explained in the following sections.

## III. COMPUTATIONAL DETAILS

The numerical work was carried out within density functional theory as implemented in the all-electron FP-LAPW code, WIEN2k [29]. As exchange- and correlation-functional, the generalized gradient approximation (GGA) in the parametrization of Perdew, Burke, and Enzerhof was chosen [30]. The angular momentum truncation was set to  $l_{\text{max}} = 9$  and  $RK_{\text{max}} = 9$ . The energy convergence criterion was set to  $10^{-5}$  Ry, whereas the charge convergence was set to  $10^{-3}$  Ry. All calculations were carried out on a  $20 \times 20 \times 20$   $k$  mesh, leading to 256 points in the irreducible wedge of the Brillouin zone.

For each compound, calculations starting with ferro- and ferrimagnetic configurations were carried out in space groups No. 225 and 216 according to the regular and inverse Heusler structure types (Fig. 1), respectively. The equilibrium lattice constant was determined through volume relaxations of the unit cell. The results of the single-point calculations for a set of different volumes was fitted to the Birch-Murnaghan equation of state, and the optimized lattice parameter was obtained. For some of the presented systems, it is known that the cubic structure is not the global energy minimum and that a tetragonal derivative exists [14,31–33]. In this stage, these structural instabilities have been ignored deferring an in-depth discussion of these instabilities to an upcoming publication.

Exchange interactions and Curie temperatures for the cubic systems were calculated using the Liechtenstein formula [34] that incorporates a “real-space” approach to the exchange interaction parameters in the Heisenberg model. The computational basis for this approach is set by the fully-relativistic SPR-KKR [35] package, which is a Green’s function-based implementation of spin-density functional theory in multiple scattering formalism. The calculations have been carried out on a complex integration grid with 48 energy points, an angular momentum truncation of  $l_{\text{max}} = 4$ , and a set of 7810  $k$ -point ensuring convergence self-consistent-field cycles.


 FIG. 2. (Color online) SP behavior for examples of (a)  $\text{Mn}_2\text{Y}^{(3d)}\text{Ga}$  and  $\text{Co}_2\text{Y}^{(3d)}\text{Ga}$  compounds and (b)  $\text{Mn}_2\text{Y}^{(4d)}\text{Ga}$  compounds.

## IV. RESULTS

### A. The Slater-Pauling rule

The results for the total magnetic moments are shown by means of an SP curve, which is valid for many of the known Heusler compounds. As seen in Fig. 2, the calculated magnetic moments for each compound in the series  $\text{Mn}_2\text{Y}^{(3d)}\text{Ga}$  are well reproduced. For compounds involving Al on the Z position, the values similarly follow the SP rule and are listed in Table I. Even for compounds formed with valence electrons less than  $N_V = 24$ , SP behavior is observed, although with

formally negative magnetic moments. The reason for this is that the minority spin count for  $N_V > 24$  is 12, which remains true for  $N_V < 24$ , albeit with a change of the spin channel, which becomes the majority spin count; this results in the formally negative moments.

For every rule, there are exceptions. For compounds with late transition metals as Y atoms (for Ni and Cu, Pd and Ag, like Pt and Au), the half-metallicity cannot be maintained.  $\text{Mn}_2\text{NiAl}$  and  $\text{Mn}_2\text{NiGa}$  are not half-metallic; however, their magnetic moments are almost integers, and thus these compounds could be mistaken for half-metallic

 TABLE I. Numerically optimized lattice parameters  $a_{\text{opt}}$  and magnetization  $M_{\text{opt}}$  of  $\text{Mn}_2$ -based Heusler alloys compared to the experimental ( $a_{\text{exp}}$ ,  $M_{\text{exp}}$ ) and theoretical ( $a_{\text{theo}}$ ,  $M_{\text{theo}}$ ) literature data.

|                          | $N_V$ | SG  | $a_{\text{opt}}$ | $M_{\text{opt}}$ | $a_{\text{exp}}$ | $M_{\text{exp}}$ | Ref.      | $a_{\text{theo}}$ | $M_{\text{theo}}$ | Ref. |
|--------------------------|-------|-----|------------------|------------------|------------------|------------------|-----------|-------------------|-------------------|------|
| $\text{Mn}_2\text{TiAl}$ | 21    | 225 | 5.96             | -2.98            |                  |                  |           | 5.96              | -2.98             | [36] |
| $\text{Mn}_2\text{VAl}$  | 22    | 225 | 5.81             | -2.00            | 5.92             | -1.94            | [37],[38] | 5.80              | -2.00             | [39] |
| $\text{Mn}_2\text{CrAl}$ | 23    | 225 | 5.73             | -1.04            |                  |                  |           | 5.71              | -1.00             | [39] |
| $\text{Mn}_3\text{Al}$   | 24    | 225 | 5.80             | 0.00             |                  |                  |           | 5.80              | 0.00              | [40] |
| $\text{Mn}_2\text{FeAl}$ | 25    | 216 | 5.76             | 1.00             |                  |                  |           | 5.73              | 1.01              | [39] |
| $\text{Mn}_2\text{CoAl}$ | 26    | 216 | 5.74             | 2.00             | 5.80             | 2.00             | [17]      | 5.75              | 2.00              | [39] |
| $\text{Mn}_2\text{NiAl}$ | 27    | 216 | 5.81             | 1.19             |                  |                  |           | 5.64              | 1.44              | [33] |
| $\text{Mn}_2\text{CuAl}$ | 28    | 216 | 5.90             | 0.20             | 5.91             | 0.22             | [41]      | 5.85              | 0.22              | [42] |
| $\text{Mn}_2\text{TiGa}$ | 21    | 225 | 5.95             | -2.97            |                  |                  |           | 5.95              | 2.98              | [36] |
| $\text{Mn}_2\text{VGa}$  | 22    | 225 | 5.82             | -1.98            | 6.10             | -1.66            | [37]      |                   |                   |      |
| $\text{Mn}_2\text{CrGa}$ | 23    | 225 | 5.76             | -1.00            |                  |                  |           | 5.71              | -1.00             | [43] |
| $\text{Mn}_3\text{Ga}$   | 24    | 225 | 5.82             | 0.01             |                  |                  | [14]      | 5.82              | 0.01              | [40] |
| $\text{Mn}_2\text{FeGa}$ | 25    | 216 | 5.76             | 1.03             |                  |                  | [31]      | 5.80              | 1.05              | [44] |
| $\text{Mn}_2\text{CoGa}$ | 26    | 216 | 5.78             | 2.00             |                  |                  |           | 5.86              |                   | [45] |
| $\text{Mn}_2\text{NiGa}$ | 27    | 216 | 5.85             | 1.18             | 5.91             |                  | [46]      |                   | 1.28              | [46] |
| $\text{Mn}_2\text{CuGa}$ | 28    | 216 | 5.94             | 0.33             |                  |                  |           | 5.94              | 0.33              | [47] |
| $\text{Mn}_2\text{ZrGa}$ | 21    | 225 | 6.14             | -3.00            |                  |                  |           |                   |                   |      |
| $\text{Mn}_2\text{NbGa}$ | 22    | 225 | 6.00             | -2.00            |                  |                  |           |                   |                   |      |
| $\text{Mn}_2\text{MoGa}$ | 23    | 225 | 5.91             | -1.01            |                  |                  |           |                   |                   |      |
| $\text{Mn}_2\text{RuGa}$ | 25    | 216 | 5.96             | 1.03             | 6.00             | 1.15             | [48]      |                   |                   |      |
| $\text{Mn}_2\text{RhGa}$ | 26    | 216 | 5.98             | 1.64             |                  |                  |           |                   |                   |      |
| $\text{Mn}_2\text{PdGa}$ | 27    | 216 | 6.12             | 0.55             |                  |                  |           |                   |                   |      |
| $\text{Mn}_2\text{AgGa}$ | 28    | 216 | 6.22             | 0.34             |                  |                  |           |                   |                   |      |

ferromagnets. Also, for  $\text{Mn}_2\text{CuAl}$ ,  $\text{Mn}_2\text{CuGa}$ ,  $\text{Mn}_2\text{PdGa}$ ,  $\text{Mn}_2\text{AgGa}$ ,  $\text{Mn}_2\text{PtGa}$ , and  $\text{Mn}_2\text{AuGa}$ , the SP behavior is no longer valid and the expected moments are smaller than those predicted by the SP rule. The moments decrease and assume noninteger values, as can be seen in Fig. 2. The reason is explained later in Sec. IV D and Figs. 6 and 8.

### B. Structure and magnetic ground state

The crystal structures for the Heusler compounds on the SP curve (SPC) occur in two different modifications. For a valence count of  $N_V \leq 24$ , the  $L2_1$  (SG 255) type is favored, whereas the  $X_a$  type (SG 216) is found for  $N_V > 24$  (see also Table I, where the results of the structural relaxation are summarized next to the known literature data for both experimental and theoretical studies of cubic alloys, if available). Comparisons with known literature values emphasize the agreement of our work with previous research in the field. Minor discrepancies are usually related to either deviations in the applied theoretical methods and details or to the comparison of high-temperature measurements with zero-temperature ground-state calculations. A disorder-induced decrease of the magnetic moments is also possible [48]. If the ground-state lattice parameters differ, so do the resulting magnetic moments.

Based on rules discussed in Sec. II and other theoretical work [39], we know that, on the one hand,  $\text{Mn}_2$ -based Heusler compounds with early transition elements on the  $Y$  position adopt the  $L2_1$ -type structure. On the other hand, compounds involving late transition metals  $Y$  adopt the  $X_a$ -type inverse Heusler structure. Table I reveals that this kind of behavior is true for all  $\text{Mn}_2$ -based Heusler compounds involving  $3d$  TMs on the  $Y$  position ( $\text{Mn}_2Y^{(3d)}\text{Ga}$ ) as well as for the  $4d$  transition metal series ( $\text{Mn}_2Y^{(4d)}\text{Ga}$ ).

Along with the structural transition, a magnetic transition from parallel to antiparallel alignment of Mn spins takes place due to Mn occupying site  $4b$ . This begins at the transition point  $N_V^C$ , where the magnetization vanishes [40]. The type of ferrimagnetic ordering changes and becomes more complex, as will be pointed out in the following section.

### C. Stability considerations and heats of formation

For estimating the stability of the investigated compounds, the heats of formation were calculated from the elemental crystals in their ground-state modification (except for Mn, where an antiferromagnetic bcc structure was used as an approximation) using total energy differences. Figure 3 shows the changes in the approximated formation energy within the series of compounds under study. One sees that the compounds are stable within the range of  $-100$  to  $-180$  kJ/mol, except for  $\text{Mn}_2\text{AgGa}$ . The existence of some compounds such as  $\text{Mn}_2\text{CoGa}$  [49] is experimentally proven through synthesis. Nevertheless, phases incorporating the investigated stoichiometries may exist in other crystal structures, such as the tetragonal derivatives of cubic Heusler structures. These findings will be presented in a later publication.

Consideration of the total energy difference between the inverse and regular structures  $\Delta E_{216-225} = E_{216} - E_{225}$  for the given chemical composition  $X_2YZ$  (Fig. 4), confirms that the  $4b$  site is going to be occupied by the earlier transition

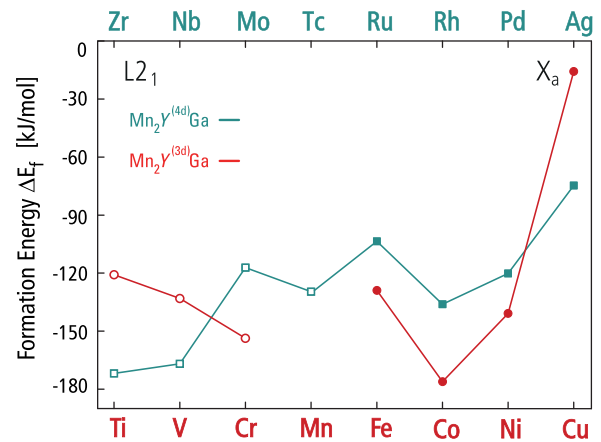


FIG. 3. (Color online) Formation energies estimated at  $T = 0$  for  $\text{Mn}_2Y^{(3d)}\text{Ga}$  and  $\text{Mn}_2Y^{(4d)}\text{Ga}$  compounds, as initial guess regarding the stability of these compounds. Open symbols denote the  $L2_1$ -type structure. Filled symbols denote the  $X_a$ -type structure.

metal among Mn and  $Y$ . This leads to the formation of the regular structures for the  $Y = \text{Ti}, \text{V}, \text{Cr}, \text{Zr}, \text{Nb}, \text{Mo}$  and inverse structures for the  $Y = \text{Fe}, \text{Co}, \text{Ni}, \text{Cu}, \text{Ru}, \text{Rh}, \text{Pd}$  and  $\text{Ag}$  containing Heusler materials. The total energy difference can be interpreted as site-preference energy for the interchange of Mn and  $Y$  that distinguishes both structure types. For instance, in  $\text{Mn}_2\text{CrGa}$ , with a rather small site-preference energy, indicating that the *regular*-type structure is not strongly preferred, thermally induced disorder is more likely to occur than, for example, for  $\text{Mn}_2\text{CoGa}$  and  $\text{Mn}_2\text{VGa}$ , with solid energy differences. Additional information about the stability of the phases under investigation was obtained from the densities of state (DOS) that are discussed in detail in the following section. It has proven useful to look for sharp peaks in the DOS at the Fermi edge that are symptoms of instabilities in the system. This applies to  $\text{Mn}_2\text{FeGa}$  [31] and  $\text{Mn}_3\text{Ga}$  [14], which have been experimentally realized in the tetragonal inverse structure. It is known that besides  $\text{Mn}_2\text{FeGa}$  and  $\text{Mn}_3\text{Ga}$  there are tetragonal phases for the  $3d$

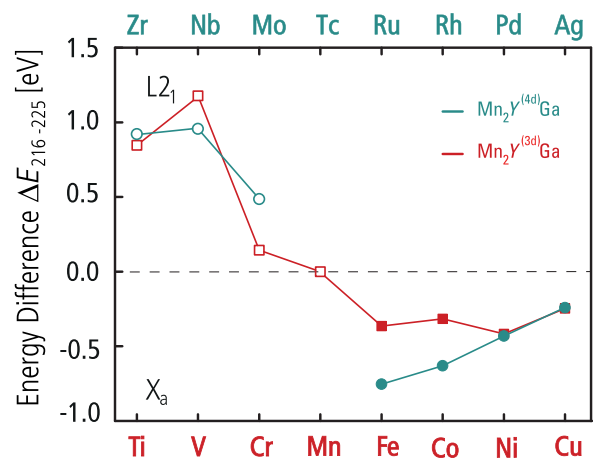


FIG. 4. (Color online) Total energy difference between the inverse and regular structures  $\Delta E_{216-225} = E_{216} - E_{225}$  calculated for  $\text{Mn}_2Y^{(3d)}\text{Ga}$  and  $\text{Mn}_2Y^{(4d)}\text{Ga}$  cubic Heusler materials.

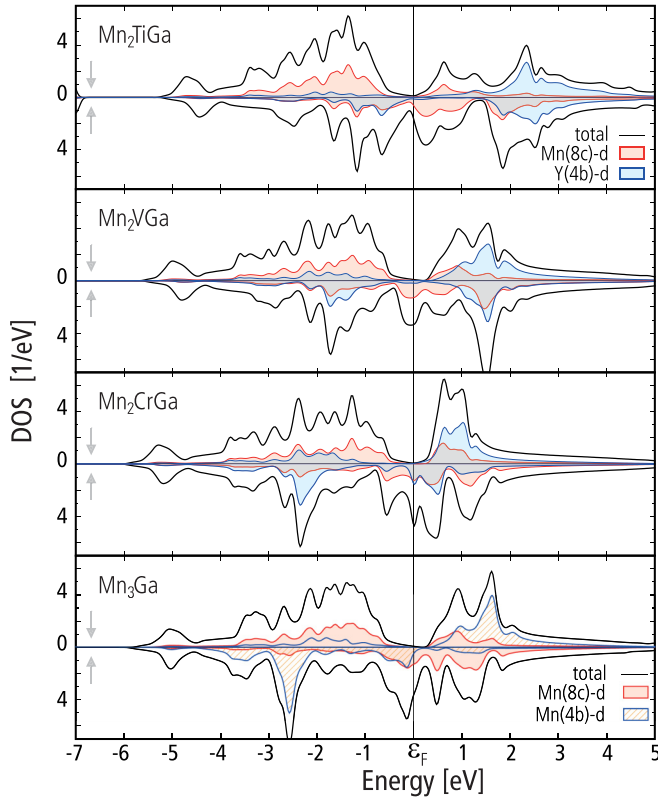


FIG. 5. (Color online) Densities of states of the  $\text{Mn}_2\text{Y}^{(3d)}\text{Ga}$  compounds with  $Y = \text{Ti}, \text{V}, \text{Cr}, \text{Mn}$ .

transition metals (TMs) involving Mn-based compounds, such as  $\text{Mn}_3\text{Al}$  and  $\text{Mn}_2\text{NiGa}$ . Furthermore, we could show that tetragonal alloys may exist in the series involving late TMs of the IV period. A detailed discussion of these phases shall be postponed to a later publication; we emphasize, however, that possible tetragonal derivatives from cubic Heusler phases do not prove their existence, as other relaxation mechanisms such as disorder phenomena may minimize the total energy. Nevertheless, the instabilities do give a strong hint, as has been seen in *ab-initio* studies related to shape-memory compounds.

#### D. Electronic structure

The calculations reveal that nearly all compounds are at least pseudo-half-metallic or even truly half-metallic with the associated gap in the *minority* densities of state (DOS) for compounds with a valence electron count of less than 24 and a gap in the *majority* DOS for more than 24 electrons. It is worth mentioning that the definition of spin-up and spin-down electrons is connected with the choice of the magnetic moment as positive. However, we may allow negative values to emphasize the occupancy of the *d* states according to the SP rule, although the notion of negative moments is unphysical. Still doing so leads to a better understanding of the mechanism of magnetic ordering. Although Figs. 5 and 6 were chosen to exhibit the gap in the spin-down channel for all compounds, the minority channel changes from the spin-down state to the spin-up state as the electron count crosses 24 electrons per formula unit.

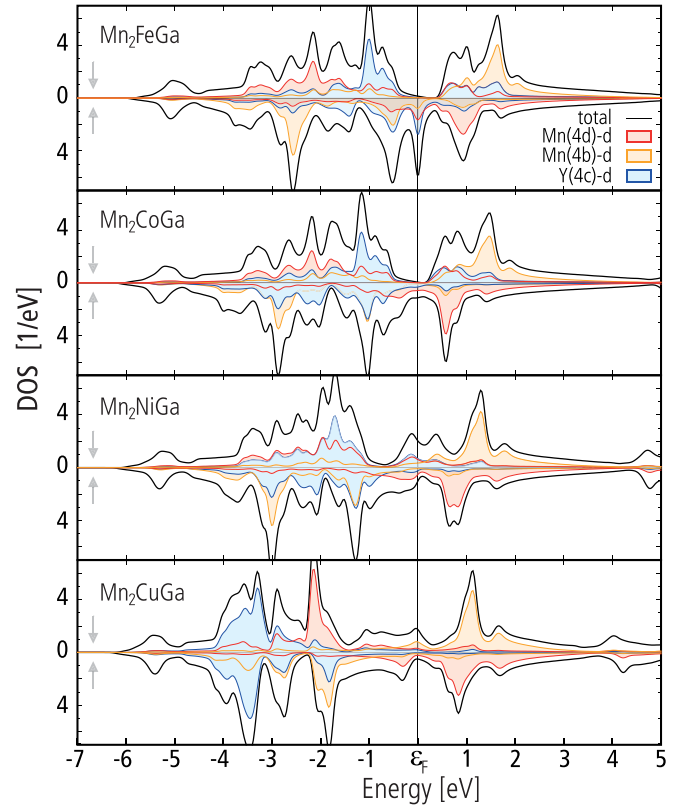


FIG. 6. (Color online) Densities of states of the  $\text{Mn}_2\text{Y}^{(3d)}\text{Ga}$  compounds with  $Y = \text{Fe}, \text{Co}, \text{Ni}, \text{Cu}$ .

In Figs. 5 and 6 (Figs. 7 and 8), the DOS for both structure types of the  $\text{MnY}^{(3d)}\text{Ga}$  ( $\text{MnY}^{(4d)}\text{Ga}$ ) series are compared. A feature seen in the DOS is that the gap at the Fermi energy is bordered by Mn states for the  $\text{L}_{21}$ -type structure, whereas this is not the case for the inverse compounds. A second property is

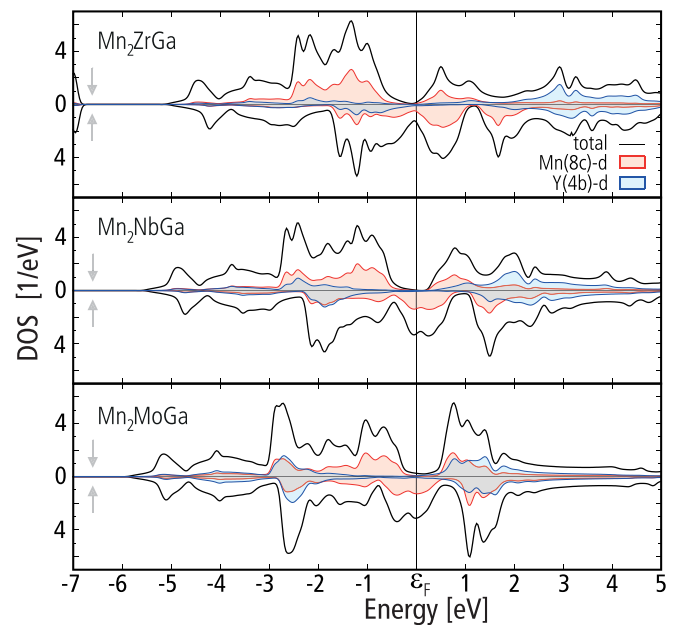


FIG. 7. (Color online) Densities of states of the  $\text{Mn}_2\text{Y}^{(4d)}\text{Ga}$  compounds with  $Y = \text{Zr}, \text{Nb}, \text{Mo}$ .

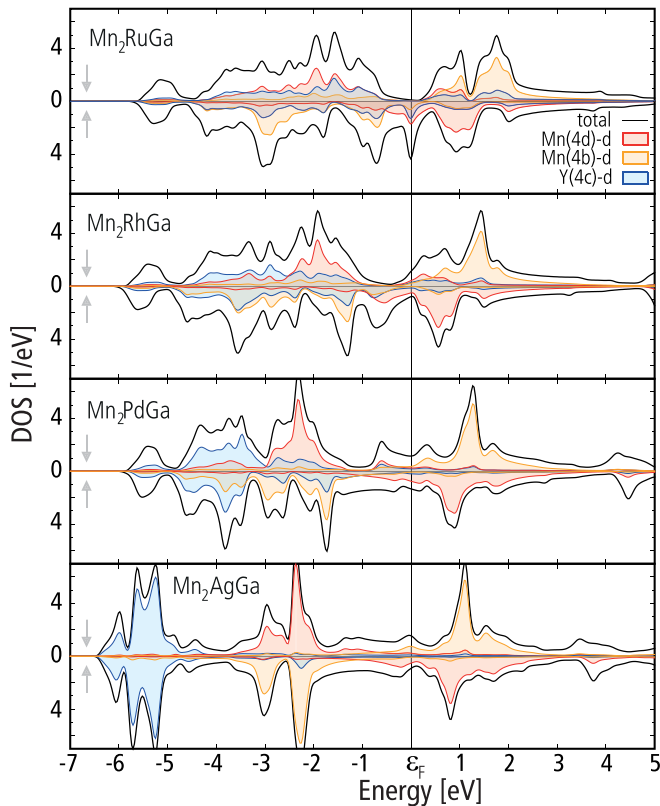


FIG. 8. (Color online) Densities of states of the  $\text{Mn}_2\text{Y}^{(4d)}\text{Ga}$  compounds with  $Y = \text{Ru, Rh, Pd, Ag}$ .

the prominent downward trend of the  $Y$   $d$  states. Independent of the structure type, the local environment of Mn exhibits tetrahedral symmetry, which leads to the SP curve being continuous across the transition point at  $N_V = 24$ , leaving the near-half metallic behavior unchanged. Following Ouardi *et al.* [50] and Galanakis *et al.* [11] the gap in the minority channel in  $\text{Mn}_2$ -based alloys is the result of hybridization of the  $X$  atoms on site  $8c$  in the SG 225, which are again tetrahedrally coordinated with their neighboring atoms. The final size of the gap is determined by the crystal field splitting of the  $e_g$  and  $t_{2g}$  states (at the  $\Gamma$  point), which is determined by the symmetry and coordination of the Mn atoms. The DOS for  $\text{Mn}_2\text{NiGa}$  and  $\text{Mn}_2\text{CuGa}$  explains the deviation from the SP curve because the gap at the Fermi energy closes. This is so because the  $d$ -electron states of Ni and Cu disappear from the Fermi energy being drawn into the core. The states at the Fermi edge are now mainly composed of  $s$  electrons for  $\text{Mn}_2\text{AgGa}$ . Condensing this finding into one number that is closely connected with the concept of half-metallicity, the spin polarization,  $P$ , emphasizes the preceding facts and is listed for the investigated compounds in Table II. Once more, the failure of the SP rule for compounds with more than 26 valence electrons is apparent in terms of the spin polarization.

### E. Local magnetic moments

A truly large number of publications on the SP behavior of various compounds exists [9,28,51], and yet the local magnetic structure has not been intensively investigated so far, even

TABLE II. The total number of the valence electrons,  $N_V$ , and valence electrons of the  $Y$  atom,  $N_{V,Y}$ , and the calculated spin polarization,  $P$ , of the DOS at the Fermi edge of the  $\text{Mn}_2\text{Y}^{(3d)}\text{Ga}$  and  $\text{Mn}_2\text{Y}^{(4d)}\text{Ga}$  series.

| $N_V$ | $N_{V,Y}$ | $\text{Mn}_2\text{Y}^{(3d)}\text{Ga}$ | $P/\%$ | $\text{Mn}_2\text{Y}^{(4d)}\text{Ga}$ | $P/\%$ |
|-------|-----------|---------------------------------------|--------|---------------------------------------|--------|
| 21    | 4         | $\text{Mn}_2\text{TiGa}$              | 83     | $\text{Mn}_2\text{ZrGa}$              | 82     |
| 22    | 5         | $\text{Mn}_2\text{VGa}$               | 94     | $\text{Mn}_2\text{NbGa}$              | 98     |
| 23    | 6         | $\text{Mn}_2\text{CrGa}$              | 97     | $\text{Mn}_2\text{MoGa}$              | 85     |
| 24    | 7         | $\text{Mn}_3\text{Ga}$                | 96     |                                       |        |
| 25    | 8         | $\text{Mn}_2\text{FeGa}$              | 95     | $\text{Mn}_2\text{RuGa}$              | 95     |
| 26    | 9         | $\text{Mn}_2\text{CoGa}$              | 93     | $\text{Mn}_2\text{RhGa}$              | 15     |
| 27    | 10        | $\text{Mn}_2\text{NiGa}$              | 35     | $\text{Mn}_2\text{PdGa}$              | 7      |
| 28    | 11        | $\text{Mn}_2\text{CuGa}$              | 53     | $\text{Mn}_2\text{AgGa}$              | 24     |

though the local magnetic structure is closely related with the magnetic phenomenon. First-principles calculations are a sophisticated tool to access site-resolved quantities such as local magnetic moments, even though the partitioning of a solid into atomic regions is an arbitrary procedure and approximate projection techniques need to be applied in most cases. But as experimental information on atomic magnetic moments in bulk Heusler materials is rather incomplete, we focus our attention on the local magnetic and electronic environment of the Mn atoms in both structure types. We show that the magnetic moment in inverse Heusler compounds ( $X_a$ ) of one Mn atom is locked at about  $3\mu_B$ , whereas no such rule is found for the local moments of the Mn-based  $L_{21}$ -type compounds, where Mn occupies the tetrahedrally coordinated position  $8c$ .

To see this, the local magnetic moments of the  $\text{Mn}_2\text{Y}^{(3d)}\text{Ga}$  and  $\text{Mn}_2\text{Y}^{(4d)}\text{Ga}$  compounds are shown in Fig. 10, while Fig. 9 provides a schematic overview of the type of magnetic order. The left-hand side of the plots Figs. 10(a) and 10(b) for  $N_V < 24$  regime displays the local moments of the transition metal atoms in the  $L_{21}$  structure. The electron count increases through the variation of the  $Y$  atom occupation from  $Y = \text{Ti}$  to  $\text{Cu}$  and from  $Y = \text{Zr}$  to  $\text{Ag}$ . As the electron count is increased by one, the magnetic moments of the systems, following the SP curve, increase by  $1\mu_B$ . Considering the series  $\text{Mn}_2\text{Y}^{(3d)}\text{Ga}$ , we recognize that the moments of  $Y(4b)$  and  $\text{Mn}(8c)$  display almost linear behavior. On the other hand, as the magnetic moment on  $Y(4b)$  increases, the absolute value of  $\text{Mn}(8c)$

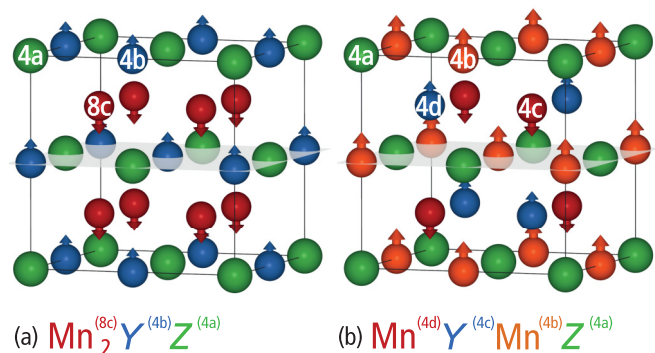


FIG. 9. (Color online) Panels (a) and (b) show the magnetic ordering as it has been obtained for the two structure types,  $L_{21}$  and  $X_a$ , respectively, with vectors indicating the magnitudes and orientation of the site magnetic moments.

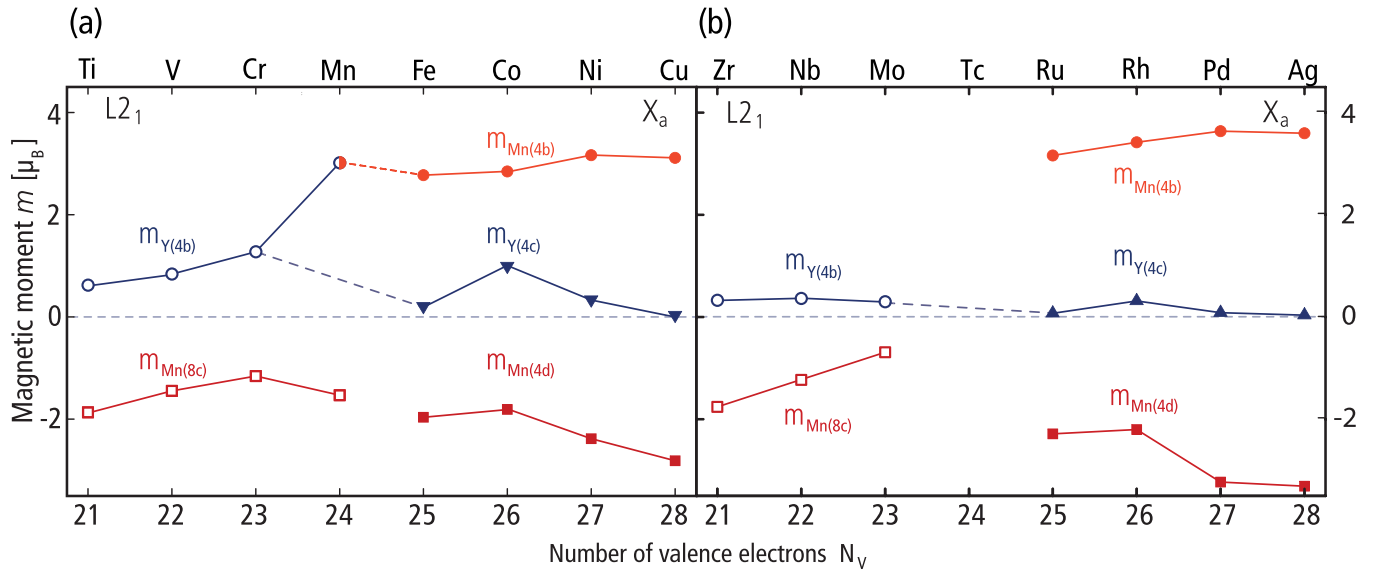


FIG. 10. (Color online) Atomic magnetic moments in (a)  $\text{Mn}_2\text{Y}^{(3d)}\text{Ga}$  and (b)  $\text{Mn}_2\text{Y}^{(4d)}\text{Ga}$  compounds. Open symbols denote the  $L2_1$ -type structure. Filled symbols denote the  $X_a$ -type structure.

decreases for both series with a change of slope at the Cr position. Increasing the electron count therefore leads to a filling of either the minority channel ( $N_V \leq 24$ ) or the majority channel ( $N_V \geq 24$ ).

As shown in Sec. IV D, every compound is at least nearly half-metallic, reflecting the change of the moments by means of the site-resolved densities of state (Fig. 5). The decreasing number of states in the minority channel and the increasing number of states in the majority channel for both Mn and Y atoms are related to the change in the local moments. Filling states of Y and Mn atoms at the same time, where the Mn magnetic moment is aligned antiparallel to the Y atom and is consequently decreasing. The trends of the  $L2_1$  Mn-based Heusler compounds intriguingly resemble the nature of the local moments in  $\text{Co}_2$ -based Heusler compounds [10].

Moving forward in the series, perhaps the most outstanding Heusler alloy,  $\text{Mn}_3\text{Ga}$ , marks the transition point between both cubic structure types. Although  $\text{Mn}_3\text{Ga}$  is found to adopt the  $L2_1$  structure in the cubic approximation, it exhibits properties of the inverse Heusler structure, namely, the antiparallel alignment of Mn atoms on sites  $4d$  and  $4b$ . The determining characteristic property of Mn-based inverse Heusler compounds clearly is this antiparallel alignment. This is displayed in Fig. 10. Through its peculiar behavior,  $\text{Mn}_3\text{Ga}$  is not only an exceptional compound of the  $L2_1$  series, but it also constitutes the *transition point* between both structure types. Additionally, the total magnetic moment for  $\text{Mn}_3\text{Ga}$  is supposed to vanish [40], as it marks the *compensation point*, following the SP rule as well. It is emphasized again that tetragonal Heusler compounds were not considered for this part of the study, and it is noted again that  $\text{Mn}_3\text{Ga}$  does not exhibit a cubic structure; as with  $\text{Mn}_3\text{Al}$ ,  $\text{Mn}_2\text{FeGa}$ ,  $\text{Mn}_2\text{NiGa}$ , and  $\text{Mn}_2\text{NiAl}$ ,  $\text{Mn}_3\text{Ga}$  has been found to be tetragonal.

With Mn occupying the  $4b$  site, the local moment on site  $4d$  increases in absolute value. But most important, the local magnetic moment of Mn on site  $4b$  is locked at  $3\mu_B$ . Although some compounds are known in the literature, a comprehensive

overview of the local magnetic structure has not been provided yet. Therefore, the remarkable consistency of the moment on site  $4b$  has not been appreciated enough.

Beyond the transition point, the magnetic ordering, following the crystallographic ordering, changes from parallel to antiparallel alignment of the Mn spins. Owing to a symmetry reduction of index  $t2$  (*translationengleiche* subgroup), the Wyckoff position  $8c$  splits into  $4d$  and  $4c$ , which are now occupied by Mn( $4d$ ) and Y( $4c$ ), the second Mn atom now occupying site  $4b$ , which is electronically distinct from site  $4d$ . The electric potential experienced on the Mn sites is different owing to the nearest neighbors, i.e., Mn( $4d$ ) is coordinated by four Ga( $4a$ ) and four Mn( $4b$ ) atoms, whereas Mn( $4b$ ) is surrounded by four Mn( $4d$ ) and four Y( $4c$ ) atoms. One observes that the nearest-neighbor combination, Mn( $4b$ )-Y( $4c$ ), results in a high local moment on Mn( $4b$ ) and ferromagnetic coupling of both species, whereas the Mn( $4b$ )-Mn( $4d$ ) coupling is antiferromagnetic, as in the elemental crystal.

While varying the Y( $4d$ ) atoms, the Y atom  $d$  states decrease in energy and act as charge sinks, leading to an increase of the magnetic moment on the Mn( $4d$ ) position owing to its atomic states and chemical environment. The character of the Y atom  $d$  state is, therefore, reflected in the energy levels of the Heusler compounds. This behavior of the magnetic moments with increasing electron count is demonstrated in Fig. 10.

The compounds shown on the right-hand side of Figs. 10(a) and 10(b) are composed by the data for the inverse compounds, and thus the contributions to the change of the total magnetic moment stem from the Mn atoms on position  $4d$  only. Meanwhile, the change in the local moments of the Y atoms is significant for Co only, whereas Fe, Ni, and Cu carry small moments that do not follow a particular trend.

Furthermore, the Mn-based Heusler compounds incorporating transition metals from the IV period are studied in the same fashion. In contrast to the series involving  $3d$  transition metals, the magnetic moments are largely built by the Mn atoms only. The contribution of the transition metals is of minor

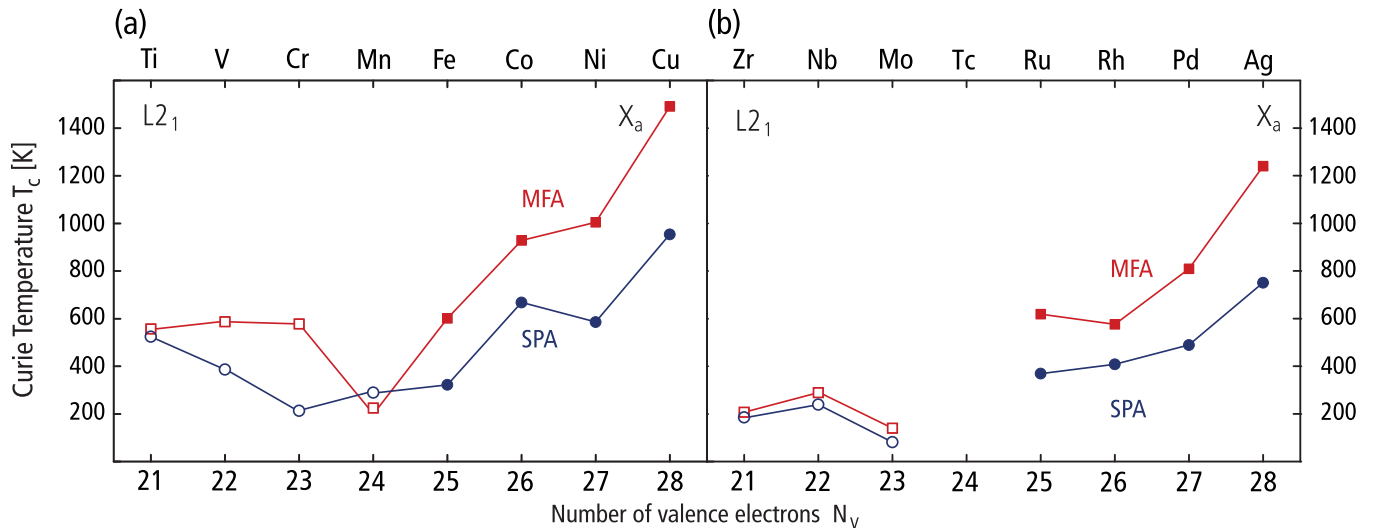


FIG. 11. (Color online) The calculated Curie temperatures of the Heusler compounds containing Ga. The results of the mean-field approximation (MFA) are compared with those of the spherical approximation (SPA). Open symbols,  $L2_1$ -type structure; filled symbols,  $X_a$ -type structure.

importance. As for the lighter homologues, the SP behavior breaks down for alloys with 27 or more valence electrons. The local magnetic moments almost compensate, as the transition metals on position  $4c$  (Pd, Ag) do not contribute to the total moment.

### F. Exchange coupling and Curie temperatures

The interaction of sites in a magnetic solid is typically parametrized on the basis of the effective Heisenberg Hamiltonian, where the interaction strength is described by the so-called exchange constants or pair interaction energies  $J_{ij}$ :  $H = -\sum_{i<j} J_{ij} \hat{e}_i \hat{e}_j$ , where  $\hat{e}_{i,j}$  are the directional unit vectors along the magnetic moments on sites  $i$  and  $j$ . Knowing the set of  $\{J_{ij}\}$ , one can estimate the magnetic order (positive  $J$  corresponds to the parallel coupling, negative  $J$  to the antiparallel one) and the ordering temperature (we will call it the Curie temperature  $T_C$  also in case of a ferrimagnet). The proper way to calculate  $T_C$  is via the exact  $T$ -dependent solutions of the parametrized Heisenberg model using Monte-Carlo simulations. In the present study, we are more interested in general trends rather than in exact solutions; therefore, we will use the standard mean-field approximation [34] (MFA), for which  $k_B T_C = 2/3 J_{\max}$ , where  $J_{\max}$  is the maximal eigenvalue of the  $\{J_0^{\mu\nu}\}$  matrix, with  $J_0^{\mu\nu} = \sum_{j \in \{\nu\}} J_{0j}$ , where 0 and  $j$  are the site indices, 0 is fixed within the  $\mu$  sublattice, and  $j$  runs over the  $\nu$  sublattice. In this case,  $J_0^{\mu\nu}$  represents the effective interaction of the 0th site from the sublattice  $\mu$  with the whole sublattice  $\nu$ . The sum over  $\nu$  sites is supposed to be infinite; in practice it is truncated at a sufficiently large cluster radius, typically a few lattice constants (in present calculations at 3.5 units of  $a$ ). Nevertheless, the single contribution to the effective exchange coupling constants are of negligible magnitude for cluster radii larger than 1.5 lattice spacings  $a$ .

For the calculation of the  $J_{ij}$  pair interactions we used Liechtenstein's real-space approach [34], which assumes that the magnetic moments and the band structure do not change when the directions of the moments are varied. Combined

with the MFA, we usually obtain a slightly overestimated  $T_C$ , which is therefore compared with a complementary formalism, the so-called spherical approximation (SPA) proposed by Moriya [52]. In the SPA the exchange interactions are obtained in reciprocal space as  $J_{\mu\nu}(\mathbf{k})$ , where  $\mu$  and  $\nu$  designate sublattice-types. For each  $\mathbf{k}$  in the Brillouin zone, all eigenvalues of the matrix  $J_{\mu\nu}(\mathbf{k})$  are obtained, calling them  $j_{n,\mathbf{k}}$ . Then  $T_C$  is estimated by means of

$$k_B T_C = \frac{2}{3} M_{\text{tot}}^2 \left[ \sum_{n,\mathbf{k}} j_{n,\mathbf{k}}^{-1} \right]^{-1}, \quad (2)$$

where  $M_{\text{tot}}^2$  is the sum of the squared local moments [9,53,54]. In contrast to the Liechtenstein formalism, this approach accounts for the change of the size of the magnetic moments upon their rotations. In practice it is found to give slightly underestimated values of  $T_C$ . The list of calculated  $T_C$  is summarized in Table V, which also contains a column with the numerical values of  $M_{\text{tot}}^2$ , the leading factor in Eq. (2). The Curie temperatures are graphed in Fig. 11 and the exchange constants in Fig. 12.

Since the differences between magnetic moments in iso-electronic  $\text{Mn}_2YZ$  with  $Z = \text{Al}$  and Ga are rather small (Table I), we will restrict further discussion to the set of  $\text{Mn}_2Y\text{Ga}$  compounds only. To understand the trends in the exchange constants and the  $T_C$  in terms of accepted concepts, Sasioglu *et al.* [55] have remarked that *ab initio* methods in general, of which DFT is just one, need to be distinguished from the model Hamiltonian approaches, which allow for the description of a single contribution to the interatomic exchange by perturbation techniques, while in the DFT used here, all types of contributions come within an effective resulting form and a more detailed analysis of the results is needed to describe the order and interaction strengths in terms of the models developed earlier, where the total exchange is split into direct and indirect contributions, i.e.,  $J_{\text{tot}} = J_{\text{direct}} + J_{\text{indirect}}$ , with different strengths and ranges.

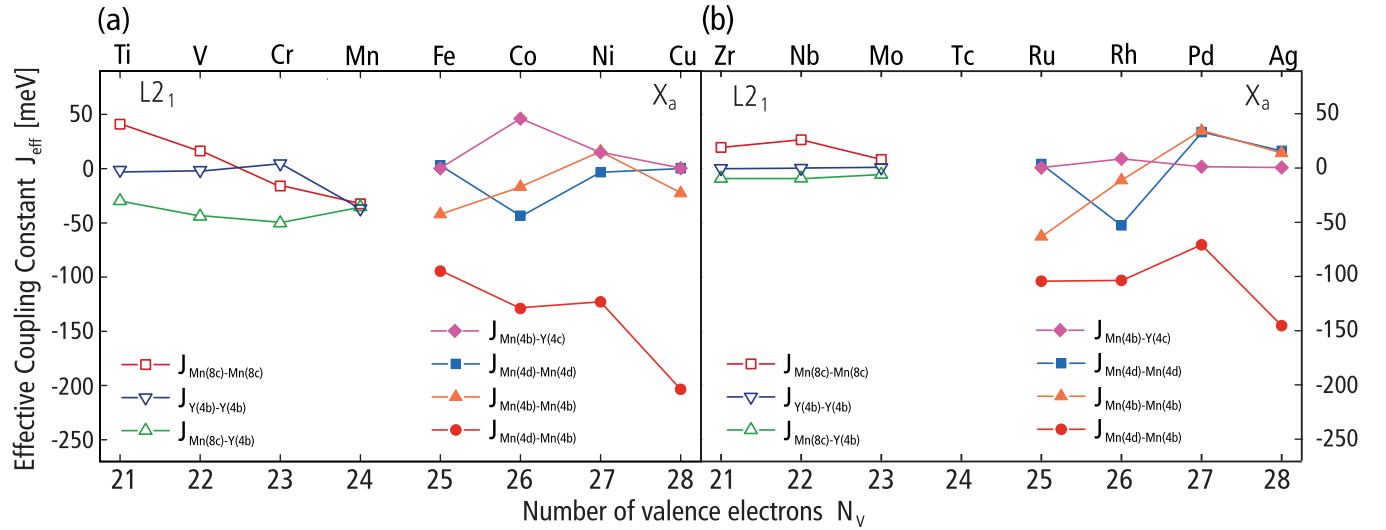


FIG. 12. (Color online) Effective exchange coupling constants  $J_0^{\mu\nu} = \sum_{j \in \nu} J_{0j}$  for the  $\text{Mn}_2\text{Y}^{(3d)}\text{Ga}$  and  $\text{Mn}_2\text{Y}^{(4d)}\text{Ga}$  compounds. Open symbols,  $L_{21}$ -type structure; filled symbols,  $X_a$ -type structure.

In Heusler compounds, such as  $\text{Pd}_2\text{MnZ}$  and  $\text{Cu}_2\text{MnZ}$ , the magnetic order is predominantly formed by the indirect Mn-Mn intrasublattice interactions  $J_{\text{indirect}}$  from a single magnetic lattice of Mn. The mediation of the exchange interactions in these compounds by the conduction  $sp$  electrons plays a crucial role described by Anderson's  $sd$  model, and  $J_{\text{indirect}}$  is phrased in terms of the Ruderman-Kittel-Kasuya-Yosida (RKKY) interaction [55]. This situation is in stark contrast to  $\text{Mn}_2\text{YZ}$  Heusler compounds that contain three magnetic sublattices. They exhibit a much more complex behavior and several types of different exchange models need to be applied.

Comparison of Figs. 11 and 12 reveals that different concepts apply to the  $L_{21}$  compounds with  $N_v < 24$  on the one hand, and the  $X_a$  compounds with  $N_v > 24$  on the other hand. The former are itinerant ferromagnets. Although exchange in these materials is mapped onto an effective Heisenberg Hamiltonian, implying interacting local moments, the itinerant nature is physically dominant. Thus, we might describe this exchange mechanism as *indirect itinerant*. The basically decreasing Curie temperatures for the increasing number of electrons (21 to 23) are due to the decreasing values of  $M_{\text{tot}}^2$ , which are given in Table V. However, the rate of the  $T_C$  change is less than that given by  $M_{\text{tot}}^2$ . This

implies that the indirect exchange grows with the number of valence electrons; see Eq. (2). The spin-polarization of the  $sp$  electrons in the  $L_{21}$  compounds [see Tables III and IV, column  $Z(4a)$ ] is opposite to the magnetization as in the  $sd$  model. It mediates the ferromagnetic order in the  $\text{Mn}(8c)$  sublattice by means of the indirect  $\text{Mn}(8c)$ - $\text{Y}(4b)$ - $\text{Mn}(8c)$  coupling [56]. The peaks occurring in the spin-up DOS indicate a certain degree of magnetic frustration that results in rather moderate interactions in contrast to the  $X_a$  compounds.

The situation is completely different for the *inverse* Heusler ( $X_a$ ) compounds with  $N_v > 24$ . Here, Mn atoms appear as the nearest neighbors, and one of them,  $\text{Mn}(4b)$  exhibits a strong localized moment, leading to another mechanism in the overall exchange. For both 3d and 4d compounds it is a short-range direct exchange that couples Mn in 4b and 4d sites antiparallel. This interaction is indicated by a pronounced negative trend in the exchange coupling constants (see Fig. 12), which becomes more negative by increasing electron number. The basically increasing  $T_C$  in both series of compounds correlate with the increasing of  $M_{\text{tot}}^2$  (see Table V). In the case of the 4d series this increase is rather regular by increasing the number of electrons, indicating no distinct changes in the exchange mechanism, which is long-range and indirect, mediated by the antiparallel 4b-4d coupling. All  $sp$  electrons are polarized

TABLE III. Atomic magnetic moments in  $\text{Mn}_2\text{Y}^{(3d)}\text{Ga}$  Heusler compounds;  $M$  is the total magnetization.

| Regular                  | $N_v$ | $a_{\text{opt}}$ | Mn(8c) | —     | Y(4b)  | Z(4a) | $M$   |
|--------------------------|-------|------------------|--------|-------|--------|-------|-------|
| $\text{Mn}_2\text{TiGa}$ | 21    | 5.95             | -1.87  |       | 0.62   | 0.05  | -2.97 |
| $\text{Mn}_2\text{VGa}$  | 22    | 5.82             | -1.45  |       | 0.84   | 0.02  | -1.98 |
| $\text{Mn}_2\text{CrGa}$ | 23    | 5.76             | -1.16  |       | 1.27   | 0.00  | -1.00 |
| $\text{Mn}_3\text{Ga}$   | 24    | 5.82             | -1.53  |       | 3.02   | 0.04  | 0.01  |
| Inverse                  | $N_v$ | $a_{\text{opt}}$ | Mn(4d) | Y(4c) | Mn(4b) | Z(4a) | $M$   |
| $\text{Mn}_2\text{FeGa}$ | 25    | 5.76             | -1.97  | 0.21  | 2.78   | 0.01  | 1.03  |
| $\text{Mn}_2\text{CoGa}$ | 26    | 5.78             | -1.81  | 1.00  | 2.85   | -0.01 | 2.00  |
| $\text{Mn}_2\text{NiGa}$ | 27    | 5.85             | -2.38  | 0.34  | 3.17   | 0.01  | 1.18  |
| $\text{Mn}_2\text{CuGa}$ | 28    | 5.94             | -2.81  | 0.04  | 3.11   | 0.00  | 0.33  |

TABLE IV. Atomic magnetic moments in  $\text{Mn}_2\text{Y}^{(4d)}\text{Ga}$  Heusler compounds;  $M$  is the total magnetization.

| Regular                  | $N_v$ | $a_{\text{opt}}$ | Mn(8c) | —     | Y(4b)  | Z(4a) | $M$   |
|--------------------------|-------|------------------|--------|-------|--------|-------|-------|
| $\text{Mn}_2\text{ZrGa}$ | 21    | 6.14             | -1.76  |       | 0.33   | 0.07  | -3.00 |
| $\text{Mn}_2\text{NbGa}$ | 22    | 6.00             | -1.23  |       | 0.36   | 0.03  | -2.00 |
| $\text{Mn}_2\text{MoGa}$ | 23    | 5.91             | -0.69  |       | 0.30   | 0.02  | -1.01 |
| Inverse                  | $N_v$ | $a_{\text{opt}}$ | Mn(4d) | Y(4c) | Mn(4b) | Z(4a) | $M$   |
| $\text{Mn}_2\text{RuGa}$ | 25    | 5.96             | -2.29  | 0.07  | 3.16   | 0.03  | 1.03  |
| $\text{Mn}_2\text{RhGa}$ | 26    | 5.98             | -2.20  | 0.31  | 3.42   | 0.03  | 1.64  |
| $\text{Mn}_2\text{PdGa}$ | 27    | 6.12             | -3.23  | 0.08  | 3.64   | 0.02  | 0.55  |
| $\text{Mn}_2\text{AgGa}$ | 28    | 6.22             | -3.31  | 0.04  | 3.60   | 0.01  | 0.34  |

TABLE V.  $T_C$  in Kelvin for  $Mn_2Y^{(3d)}Ga$ ,  $Mn_2Y^{(3d)}Al$  and  $Mn_2Y^{(4d)}Ga$  Heusler compounds. Present calculations using MFA and SPA formalisms are referred as  $T_{C,MFA}$  and  $T_{C,SPA}$ ; the values from the literature  $T_{C,lit}$  are marked by the subscripts “t” or “e”, which refer to theoretical calculations and experimental measurements, respectively.  $M_{tot}^2$  in  $\mu_B^2$  is the sum of the squared local moments, Eq. (2).

| Material   | $T_{C,MFA}$ | $T_{C,SPA}$ | $T_{C,lit}$  | $M_{tot}^2$ | Ref.           |
|------------|-------------|-------------|--|-------------|----------------|
| $Mn_2TiGa$ | 557         | 525         | 663 <sub>t</sub>                                       | 7.4         | [36]           |
| $Mn_2VGa$  | 587         | 387         | 783 <sub>e</sub>                                       | 4.9         | [57]           |
| $Mn_2CrGa$ | 578         | 213         |  | 4.3         |                |
| $Mn_3Ga$   | 225         | 290         | 482 <sub>t</sub>                                       | 13.8        | [54]           |
| $Mn_2FeGa$ | 601         | 322         |  | 11.6        |                |
| $Mn_2CoGa$ | 928         | 668         | 710 <sub>e</sub> , 886 <sub>t</sub>                    | 12.4        | [49],[45]      |
| $Mn_2NiGa$ | 1005        | 586         | 600 <sub>e</sub>                                       | 15.8        | [58]           |
| $Mn_2CuGa$ | 1491        | 954         |  | 17.6        |                |
| $Mn_2ZrGa$ | 207         | 185         |  | 6.3         |                |
| $Mn_2NbGa$ | 289         | 239         |  | 3.2         |                |
| $Mn_2MoGa$ | 140         | 81          |  | 1.0         |                |
| $Mn_2RuGa$ | 619         | 369         | 560 <sub>e</sub>                                       | 15.2        | [48]           |
| $Mn_2RhGa$ | 576         | 408         |  | 16.6        |                |
| $Mn_2PdGa$ | 809         | 490         |  | 23.6        |                |
| $Mn_2AgGa$ | 1240        | 751         |  | 23.9        |                |
| $Mn_2TiAl$ | 428         |             | 665  | 7.15        | [36]           |
| $Mn_2VAl$  | 588         |             | 663 <sub>t</sub> , 638 <sub>t</sub> , 760 <sub>e</sub> | 4.72        | [54],[56],[57] |
| $Mn_2CrAl$ | 549         |             |  | 3.16        |                |
| $Mn_3Al$   | 306         | 196         |  | 12.02       |                |
| $Mn_2FeAl$ | 614         | 200         |  | 10.33       |                |
| $Mn_2CoAl$ | 985         | 740         | 720 <sub>e</sub> , 890 <sub>t</sub>                    | 10.54       | [17],[45]      |
| $Mn_2NiAl$ | 1140        | 452         |  | 13.40       |                |
| $Mn_2CuAl$ | 1539        | 884         |  | 14.85       |                |

parallel to the localized moments of  $Mn(4b)$  as can be inferred from Table IV. The trend in the  $3d$  series is similar but less regular because of the relatively large magnetic moment of Co. Table III reveals a sign change in the spin-polarization of the  $sp$  electrons. This might be the reason for the boost in the indirect exchange interaction that reveals in the exceptionally large  $T_C$  of  $Mn_2CoGa$ . This is also true for  $Mn_2CoAl$  as can be seen in Table V.

## V. SUMMARY

The SP curves show that the magnetic moments of Mn-based compounds, independent of the structure type, are continuous across the compensation point and follow the

SP rule (with the exception of compounds with  $N_V \geq 27$ ). The total magnetization  $M$  is composed of contributions of different characters (localized or itinerant) for the different structure types (Figs. 10 and 12). Considering the empirical rules regarding the chemical ordering (Sec. II) and accounting for the trends in the local moments, we can understand how the magnetization in  $Mn_2YZ$  systems is formed. The  $L2_1$ -type Heusler compounds are itinerant ferrimagnets with small magnetic moments on the Mn atoms that are coupled ferromagnetically. The  $Y$  atoms on  $4b$  sites are of minor importance in the sum of the various contributions to the total moment. They are coupled antiparallel to the Mn moments on the  $8c$  sites. The magnetism in the  $X_a$ -type (inverse) Heusler compounds is composed of a large, localized [2,59] system-independent moment on  $Mn(4b)$  of about  $3\mu_B$ . The magnetic moment of  $Mn(4d)$  increases in absolute value, whereas the  $Y$  atoms, with the exception of Co, contribute small moments in both structure types. Even for the compounds that do not follow the SP rule ( $Mn_2NiGa$ ,  $Mn_2CuGa$ ,  $Mn_2RuGa$ ,  $Mn_2RhGa$ ,  $Mn_2PdGa$ ), the trends regarding the local moments are still valid. Regarding the large constant localized moment, Mn is thus the only  $3d$  transition metal element in inverse Heusler compounds that behaves like a rare-earth element.

The calculated exchange constants give an estimate of Curie temperatures in two different approximations that are likely to border the experimental values. Figure 11 can be separated into the  $L2_1$  and  $X_a$  parts. In  $L2_1$ , the Curie temperatures show only little variation. Starting with the materials with  $N_V = 24$  ( $X_a$  transition point), care has to be taken with these values because of the occurrence of a phase change to tetragonal structures for some compounds. If the compounds remain in the cubic structure, the trend shown indicates an increase in the Curie temperature with increasing electron numbers owing to the increase of the local moments at roughly constant exchange interactions. The latter can be attributed to indirect exchange, which can either be of Ruderman-Kittel type [55] or of the Zener-DeGennes [60,61] variant. We believe the antiferromagnetic coupling of the two types of Mn atoms in the inverse Heusler compounds is due to direct exchange being an atomic property of Mn as in the elementary metal; the half-filled  $d$  shell leads to antiparallel coupling.

## ACKNOWLEDGMENTS

The authors gratefully acknowledge financial support from Project P 1.2-A of research unit FOR 1464 “ASPIMATT” and the European Research Council Advanced Grant (ERC-AG) No. 291472 “IDEA Heusler!”

- [1] R. A. de Groot, F. M. Mueller, P. G. van Engen, and K. H. J. Buschow, *Phys. Rev. Lett.* **50**, 2024 (1983).
- [2] J. Kübler, A. R. Williams, and C. B. Sommers, *Phys. Rev. B* **28**, 1745 (1983).
- [3] T. Block, C. Felser, G. Jakob, J. Ensling, B. Mühling, P. Gütlich, and R. J. Cava, *J. Solid State Chem.* **176**, 646 (2003).
- [4] C. Felser and G. H. Fecher, *Spintronics: From Materials to Devices* (Springer, Berlin/Heidelberg, 2013).
- [5] H. Liu, Y. Honda, T. Taira, K. Matsuda, M. Arita, T. Uemura, and M. Yamamoto, *Appl. Phys. Lett.* **101**, 132418 (2012).
- [6] M. Bowen, M. Barthélémy, M. Bibes, E. Jacquet, J. Contour, A. Fert, D. Wortmann, and S. Blügel, *J. Phys.: Condens. Matter* **17**, L407 (2005).
- [7] K. E. H. M. Hanssen, P. E. Mijnders, L. P. L. M. Rabou, and K. H. J. Buschow, *Phys. Rev. B* **42**, 1533 (1990).
- [8] M. Jourdan, J. Minár, J. Braun, A. Kronenberg, S. Chadov, B. Balke, A. Gloskovskii, M. Kolbe, H. J. Elmers, G. Schönhense, H. Ebert, C. Felser, and M. Kläui, *Nat. Commun.* **5**, 3974 (2014).
- [9] J. Kübler, G. H. Fecher, and C. Felser, *Phys. Rev. B* **76**, 024414 (2007).

- [10] H. C. Kandpal, G. Fecher, and C. Felser, *J. Phys. D: Appl. Phys.* **40**, 1507 (2007).
- [11] I. Galanakis, P. H. Dederichs, and N. Papanikolaou, *Phys. Rev. B* **66**, 174429 (2002).
- [12] J. Winterlik, S. Chadov, A. Gupta, V. Alijani, T. Gasi, K. Filsinger, B. Balke, G. H. Fecher, C. A. Jenkins, F. Casper, J. Kübler, G.-D. Liu, L. Gao, S. S. P. Parkin, and C. Felser, *Adv. Materials* **24**, 6283 (2012).
- [13] J. Slonczewski, *J. Magn. Magn. Materials* **159**, L1 (1996).
- [14] B. Balke, G. H. Fecher, J. Winterlik, and C. Felser, *Appl. Phys. Lett.* **90**, 152504 (2007).
- [15] F. Wu, S. Mizukami, D. Watanabe, H. Naganuma, M. Oogane, Y. Ando, and T. Miyazaki, *Appl. Phys. Lett.* **94**, 122503 (2009).
- [16] J. Winterlik, B. Balke, G. H. Fecher, C. Felser, M. C. M. Alves, F. Bernardi, and J. Morais, *Phys. Rev. B* **77**, 054406 (2008).
- [17] S. Ouardi, G. H. Fecher, C. Felser, and J. Kübler, *Phys. Rev. Lett.* **110**, 100401 (2013).
- [18] J. Sticht, K.-H. Höck, and J. Kübler, *J. Phys.: Condens. Matter* **1**, 8155 (1989).
- [19] E. Krén and G. Kádár, *Solid State Commun.* **8**, 1653 (1970).
- [20] H. Niida, T. Hori, and Y. Nakagawa, *J. Phys. Soc. Japan* **52**, 1512 (1983).
- [21] H. Kurt, K. Rode, M. Venkatesan, P. S. Stamenov, and J. M. D. Coey, *Phys. Rev. B* **83**, 020405(R) (2011).
- [22] H. Kurt, N. Baadji, K. Rode, M. Venkatesan, P. S. Stamenov, S. Sanvito, and J. M. D. Coey, *Appl. Phys. Lett.* **101**, 132410 (2012).
- [23] T. Graf, C. Felser, and S. S. P. Parkin, *Progr. Solid State Chem.* **39**, 1 (2011).
- [24] J. C. Slater, *Phys. Rev.* **49**, 931 (1936).
- [25] L. Pauling, *Phys. Rev.* **54**, 899 (1938).
- [26] J. Friedel, *Il Nuovo Cim.* **7**, 287 (1958).
- [27] J. Kübler, *Physica B+C* **127**, 257 (1984).
- [28] S. Skaftouros, K. Ozdogan, E. Sasioglu, and I. Galanakis, *Phys. Rev. B* **87**, 024420 (2013).
- [29] P. Blaha, K. Schwarz, G. K. H. Madsen, D. Kvasnicka, and J. Luitz, *WIEN2k, An Augmented Plane Wave + Local Orbitals Program for Calculating Crystal Properties* (Karlheinz Schwarz, Techn. Universitat Wien, Austria, 2001).
- [30] J. P. Perdew, K. Burke, and M. Ernzerhof, *Phys. Rev. Lett.* **77**, 3865 (1996).
- [31] T. Gasi, A. K. Nayak, J. Winterlik, V. Ksenofontov, P. Adler, M. Nicklas, and C. Felser, *Appl. Phys. Lett.* **102**, 202402 (2013).
- [32] G. D. Liu, J. L. Chen, Z. H. Liu, X. F. Dai, G. H. Wu, B. Zhang, and X. X. Zhang, *Appl. Phys. Lett.* **87**, 262504 (2005).
- [33] H. Luo, G. Liu, F. Meng, S. Li, W. Zhu, G. Wu, X. Zhu, and C. Jiang, *Physica B* **405**, 3092 (2010).
- [34] A. I. Liechtenstein, M. I. Katsnelson, P. V. Antropov, and A. V. Gubanov, *J. Magn. Magn. Materials* **67**, 65 (1987).
- [35] H. Ebert, D. Ködderitzsch, and J. Minár, *Rep. Prog. Phys.* **74**, 096501 (2011).
- [36] M. Meinert, J. Schmalhorst, and G. Reiss, *J. Phys.: Condens. Matter* **23**, 036001 (2011).
- [37] K. H. J. Buschow and P. G. van Engen, *J. Magn. Magn. Materials* **25**, 90 (1981).
- [38] C. Jiang, M. Venkatesan, and J. M. D. Coey, *Solid State Commun.* **118**, 513 (2001).
- [39] H. Luo, Z. Zhu, L. Ma, S. Xu, X. Zhu, C. Jiang, H. Xu, and G. Wu, *J. Phys. D: Appl. Phys.* **41**, 055010 (2008).
- [40] S. Wurmehl, H. C. Kandpal, G. H. Fecher, and C. Felser, *J. Phys.: Condens. Matter* **18**, 6171 (2006).
- [41] Z. Q. Feng, H. Z. Luo, Y. X. Wang, Y. X. Li, W. Zhu, G. H. Wu, and F. B. Meng, *Phys. Stat. Sol. (a)* **207**, 1481 (2010).
- [42] S. T. Li, Z. Ren, X. H. Zhang, and C. M. Cao, *Physica B* **404**, 1965 (2009).
- [43] H. Luo, Z. Zhu, G. Liu, S. Xu, G. Wu, H. Liu, J. Qu, and Y. Li, *J. Magn. Magn. Materials* **320**, 421 (2008).
- [44] H. Z. Luo, H. W. Zhang, Z. Y. Zhu, L. Ma, S. F. Xu, G. H. Wu, X. X. Zhu, C. B. Jiang, and H. B. Xu, *J. Appl. Physics* **103**, 083908 (2008).
- [45] M. Meinert, J.-M. Schmalhorst, and G. Reiss, *J. Phys.: Condens. Matter* **23**, 116005 (2011).
- [46] G. D. Liu, X. F. Dai, S. Y. Yu, Z. Y. Zhu, J. L. Chen, G. H. Wu, H. Zhu, and J. Q. Xiao, *Phys. Rev. B* **74**, 054435 (2006).
- [47] A. Chakrabarti, M. Siewert, T. Roy, K. Mondal, A. Banerjee, M. E. Gruner, and P. Entel, *Phys. Rev. B* **88**, 174116 (2013).
- [48] T. Hori, M. Akimitsu, H. Miki, K. Ohoyama, and Y. Yamaguchi, *Appl. Phys. A* **74**, 737 (2002).
- [49] G. J. Li, E. K. Liu, H. G. Zhang, J. F. Qian, H. W. Zhang, J. L. Chen, W. H. Wang, and G. H. Wu, *Appl. Phys. Lett.* **101**, 102402 (2012).
- [50] S. Ouardi, G. H. Fecher, B. Balke, A. Beleanu, X. Kozina, G. Stryganyuk, C. Felser, W. Klöß, H. Schrader, F. Bernardi, J. Morais, E. Ikenaga, Y. Yamashita, S. Ueda, and K. Kobayashi, *Phys. Rev. B* **84**, 155122 (2011).
- [51] I. Galanakis and P. H. Dederichs, in *Half-metallic Alloys*, Lecture Notes in Physics, Vol. 676, edited by I. Galanakis and P. Dederichs (Springer, Berlin/Heidelberg, 2005), pp. 1–39.
- [52] T. Moriya, *Spin Fluctuations in Itinerant Electron Magnetism*, Springer Series in Solid-State Sciences No. 56 (Springer, Berlin/Heidelberg, 1985).
- [53] J. Kübler, *Theory of Itinerant Electron Magnetism* (Oxford University Press, Oxford, 2000; revised edition, 2009).
- [54] J. Kübler, *J. Phys.: Condens. Matter* **18**, 9795 (2006).
- [55] E. Sasioglu, L. M. Sandratskii, and P. Bruno, *Phys. Rev. B* **77**, 064417 (2008).
- [56] E. Sasioglu, L. M. Sandratskii, and P. Bruno, *J. Phys.: Condens. Matter* **17**, 995 (2005).
- [57] K. R. Kumar, J. A. Chelvane, G. Mark, G. Markandeyulu, S. K. Malik, and N. H. Kumar, *Solid State Commun.* **150**, 70 (2010).
- [58] C. G. F. Blum, S. Ouardi, G. H. Fecher, B. Balke, X. Kozina, G. Stryganyuk, S. Ueda, K. Kobayashi, C. Felser, S. Wurmehl, and B. Büchner, *Appl. Phys. Lett.* **98**, 252501 (2011).
- [59] M. Meinert, J.-M. Schmalhorst, C. Klewe, G. Reiss, E. Arenholz, T. Böhnert, and K. Nielsch, *Phys. Rev. B* **84**, 132405 (2011).
- [60] C. Zener, *Phys. Rev.* **82**, 403 (1951).
- [61] P. G. de Gennes, *Phys. Rev.* **118**, 141 (1960).